

## Supplementary Information

# Elementary Steps in the Formation of Hydrocarbons from Surface Methoxy Groups in HZSM-5 seen by Synchrotron Infrared Microspectroscopy

Ivalina B. Minova,<sup>a</sup> Santhosh K. Matam,<sup>b,c</sup> Alex Greenaway,<sup>b</sup> C. Richard A. Catlow,<sup>b,c,d</sup> Mark D. Frogley,<sup>e</sup> Gianfelice Cinque,<sup>e</sup> Paul A. Wright,<sup>a</sup> Russell F. Howe.<sup>f\*</sup>

<sup>a</sup> EastCHEM School of Chemistry, University of St Andrews, St Andrews KY16 9ST

<sup>b</sup> UK Catalysis Hub, Research Complex at Harwell, STFC Rutherford Appleton Laboratory, Didcot, Oxon OX11 0FA

<sup>c</sup> Cardiff Catalysis Institute, School of Chemistry, Cardiff University, Cardiff CF10 1AT

<sup>d</sup> Department of Chemistry, University College London, 20 Gower St., London WC1E 6BT

<sup>e</sup> Diamond Light Source, Harwell Science and Innovation Campus, Didcot, OX11 0DE

<sup>f</sup> Chemistry Department, University of Aberdeen, AB24 3UE

\* Correspondence to this author at r.howe@abdn.ac.uk

## Table of Contents

S1 Synthesis and Characterisation of HZSM-5 Single Crystals for Operando IR Microspectroscopy .....	2
S2 Microreactor Catalytic Data for the HZSM-5 Crystals.....	7
S3 Experimental Details of Synchrotron Measurements.....	8
S4 Supplementary Infrared Spectra and MS Data .....	10
References .....	19

## **S1: Synthesis and Characterisation of HZSM-5 Single Crystals for *Operando* IR Microspectroscopy.**

Large coffin-shaped crystals of aluminosilicate HZSM-5 were prepared as twinned tablets by a modification of the procedures utilised by Guth *et al.*<sup>1</sup> and Losch *et al.*<sup>2</sup>. The method relies on the slow dissolution of fumed silica in ammonium fluoride media under hydrothermal conditions. Tetrapropylammonium bromide (TPABr, 98%), NH<sub>4</sub>F (98%), Al(NO<sub>3</sub>)<sub>3</sub>·9H<sub>2</sub>O (98%), and fumed silica (0.2–0.3 μm), were sourced from Sigma Aldrich and used without further purification, deionised water was produced on site. TPABr (0.27 g, 1.0 mmol), NH<sub>4</sub>F (0.28 g, 7.4 mmol), Al(NO<sub>3</sub>)<sub>3</sub>·9H<sub>2</sub>O (0.19 g, 0.7 mmol) were added to deionised water (9.00 g, 500 mmol) and fumed silica (0.60 g, 10 mmol) was slowly added. The gel (100 SiO<sub>2</sub> : 5 Al(NO<sub>3</sub>)<sub>3</sub>·9H<sub>2</sub>O : 75 NH<sub>4</sub>F : 5000 H<sub>2</sub>O : 9 TPABr) was stirred at room temperature for 2 hours before being sealed in a Teflon lined autoclave (30 mL, Parr) and heated at 463 K for 10 days in a static oven. The solid was recovered by vacuum filtration, washed with deionised water and dried overnight at 373 K. Prior to spectroscopic measurements, the crystals were freshly calcined by heating at 823 K (2 °K/min) in oxygen for 64 hours.

### **Characterisation Techniques Employed.**

XRF analysis on selected samples was obtained at the Johnson Matthey Chilton site. The sample was mixed with a lithium-based flux mixture and fused into a bead at temperature above 1000 °C. The wt.% of the elements present were determined with the help of a WD spectrometer equipped with a Panalytical Axios 4 kW rhodium tube X-ray generator.

Scanning Electron Micrographs were obtained from a JEOL JSM-5600 SEM. Electron dispersive X-ray (EDS) analysis was obtained on the same instrument using the Oxford INCA Energy 200 EDS.

Cross-sectional SEM-EDS measurements were obtained by Hans J. Bongard at the Max-Planck-Institut für Kohlenforschung Department of Heterogeneous Catalysis using EDS analysis on a high resolution scanning electron microscope (Hitachi S-5500) with a point resolution of up to 4 Å at 30 kV. Ar-ion milling was used to cleave the crystal and study the elemental composition from the entire cross section of the crystal.

Solid-state magic angle spinning nuclear magnetic resonance experiments were performed at the University of St Andrews on selected samples using a Brüker Advance III 400 MHz spectrometer equipped with a 9.4 T widebore superconducting magnet. Prior to obtaining quantitative <sup>27</sup>Al MAS NMR, the sample was left to hydrate overnight in a water-containing desiccator.

To characterise the number of acid sites and their strength, temperature-programmed ammonia desorption (NH<sub>3</sub>-TPD) was performed using a Micrometrics AutoChem 2920 coupled to a Pfeiffer Vacuum ThermoStar™ quadrupole mass spectrometer. For each experiment, 100 mg of zeolite sample was loaded into the U-shaped quartz reactor, equipped with a thermocouple and quartz wool plug, which was placed inside a furnace. The zeolite was dehydrated following a two stage process by heating at 393 K (10 K min<sup>-1</sup>), and then at 673 K for 120 minutes under Ar. After cooling to 383 K, the gas flow was switched to a 15% NH<sub>3</sub> in He (25 mL min<sup>-1</sup>) for 60 min. The reactor chamber was then flushed with Ar for 60 min at 383 K to remove any excess NH<sub>3</sub> before monitoring desorption. Ammonia was desorbed with a gradual temperature increase from 382 K to 1073 K (10 K min<sup>-1</sup>). The catalyst was held at 1073 K for 30 min to ensure all of the ammonia was desorbed. The total

amount of ammonia desorbed during the heating ramp was monitored by mass spectrometry ( $m/z$  17) and  $\text{Co}(\text{NH}_3)_6\text{Cl}_3$  was used as calibration standard.

$\text{N}_2$  adsorption-desorption isotherm were measured volumetrically on a Micrometrics Tristar after dehydrating the sample under vacuum at 473 K overnight.

Calcined single crystals (150 mg) were mixed with quartz (150 mg) and tested for the dimethylether-to-hydrocarbons reaction using a Salamander fixed-bed microreactor. A continuous flow of dimethylether ( $5 \text{ mL min}^{-1}$ ) diluted in nitrogen gas ( $100 \text{ mL min}^{-1}$ ) was passed over the catalytic bed for five minutes. The DME/ $\text{N}_2$  flow rate used is equivalent to a hydrocarbon WHSV of  $3.78 \text{ h}^{-1}$ . Gas phase products were directed to an on-line gas chromatograph (Agilent GC) for separation and analysis. The GC was equipped with a capillary GC GasPro column ( $0.32 \text{ mm} \times 30 \text{ m}$ ) using Flame Ionisation Detector (FID).

### Characterisation of HZSM-5 Crystals.

The crystals grew with a homogeneous crystal size and usual ‘hour-glass’ sectoring, evident under polarised light (Figure S1). After calcination, the purity of the H-ZSM-5 material obtained was confirmed by diffraction (Figure S2). The crystal dimensions were determined from the SEM image in Figure S3. Analysis of the Si:Al ratio from XRF, EDS and  $\text{NH}_3$ -TPD analysis estimates about four Al atoms per unit cell (Table S1), which is in agreement with four  $\text{TPA}^+$  structure directing agent molecules estimated from CHN (8.9 wt.% C, 1.7 wt.% H, 1.07 wt.% N) and TGA analysis (14 wt.% loss).

**Table S1.** Characterisation of HZSM-5 Crystal.

Crystal size ( $a \times b \times c$ ) in microns	$\sim 60 \times 60 \times 160$
Si:Al (surface EDS)	$31 \pm 3$
Si:Al (cross section EDS)	$25 \pm 3$
Si:Al ( $\text{NH}_3$ -TPD)	21
Si:Al (XRF)	27
Pore volume and surface area ( $\text{N}_2$ adsorption)	$0.19 \text{ cm}^3 \text{ g}^{-1}$ $\sim 350 \text{ m}^2 \text{ g}^{-1}$

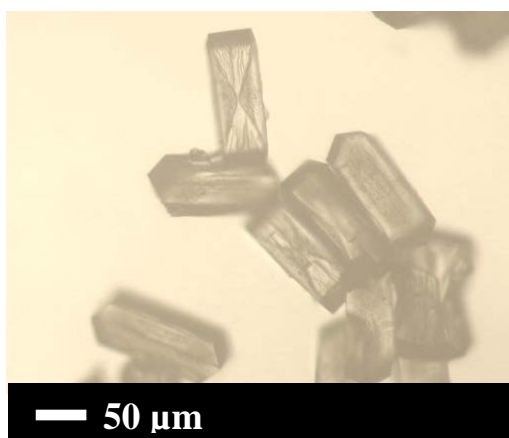


**Figure S1.** Optical image of the as-prepared ZSM-5 crystals.

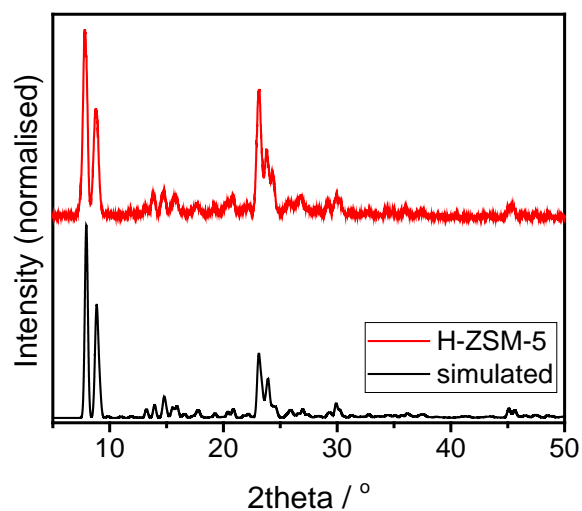


**Figure S2.** Capillary XRD data of the calcined HZSM-5 compared to the simulated pattern of HZSM-5 (Atlas structural data).

The distribution of Al was also characterised by cleaving the crystals and performing an EDS line scan across the exposed cross section (Figure S4). A homogeneous distribution of Al was found in contrast to other cases for large crystals of HZSM-5 with a deficient quantity of Al in the core.<sup>3,4</sup> A homogeneous distribution of Al is attributed to the use of  $\text{NH}_4\text{F}$  rather than  $\text{NH}_4\text{OH}$  in the synthesis gel.

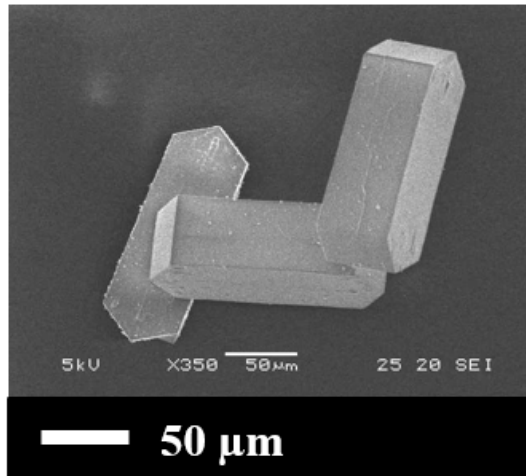


**Figure S3.** SEM image of calcined crystals of ZSM-5.

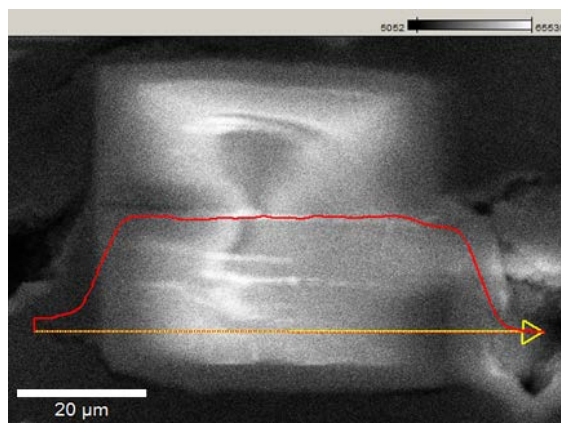


**Figure S4.** Electron microprobe analysis across a cleaved HZSM-5 crystal. The red line indicates the quantity of Al across the inner core of the crystal.

The bulk sample was ground and analysed by  $^{27}\text{Al}$  MAS NMR and  $^{29}\text{Si}$  MAS NMR. The strong narrow resonance at ca. 53–56 ppm in the calcined material is typical of the tetrahedrally-coordinated aluminium in HZSM-5.<sup>5,6</sup>

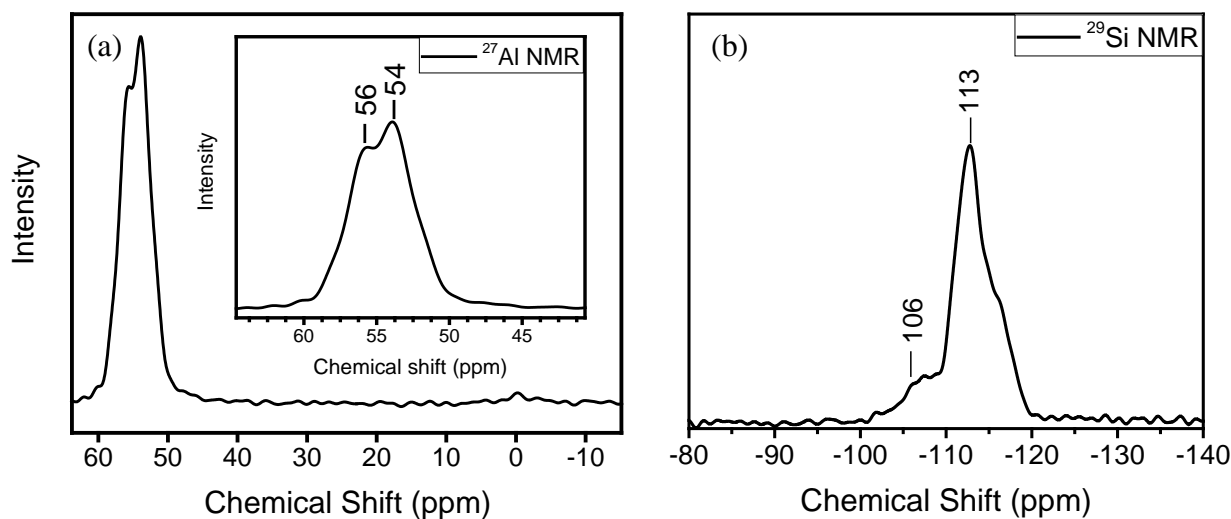


**Figure S5.** (a)  $^{27}\text{Al}$  MAS NMR (400 MHz) and (b)  $^{29}\text{Si}$  MAS NMR (400 MHz) of ground HZSM-5 crystals, calcined and hydrated.

The crystals contain  $0.8 \pm 0.1 \text{ mmol g}^{-1}$  concentrations of strong acid sites as estimated from the area of the high temperature ammonia desorption peak (HTP) at 693 K.

The calcined crystals are porous as shown by nitrogen adsorption volumetric analysis (Figure S6).

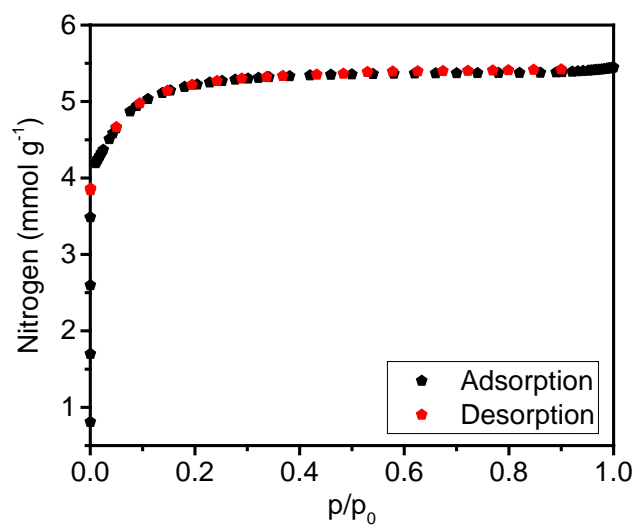


**Figure S6.** Nitrogen adsorption and desorption isotherms of HZSM-5 at 77 K.

## S2. Microreactor Catalytic Data for the HZSM-5 Crystals.

To confirm that the calcined ZSM-5 crystals were catalytically active for hydrocarbon formation their activity was tested for dimethylether conversion in a conventional microreactor. A mixture of hydrocarbons (ethene, propene, butenes, pentenes, hexenes and aromatics) similar to the trace of a commercial catalyst were produced with a high selectivity to propene after a 5 min time-on-stream in the 573–673 K temperature range tested (Figure S7). This high selectivity to propene is typical of HZSM-5 during the initial stages of the reaction. Mass balance of the sample weight before and after calcination suggested no significant amounts of coke present (< 0.1%) after calcination. At longer times (over 1 hour) catalyst conversion rate declined significantly due to coke formation.

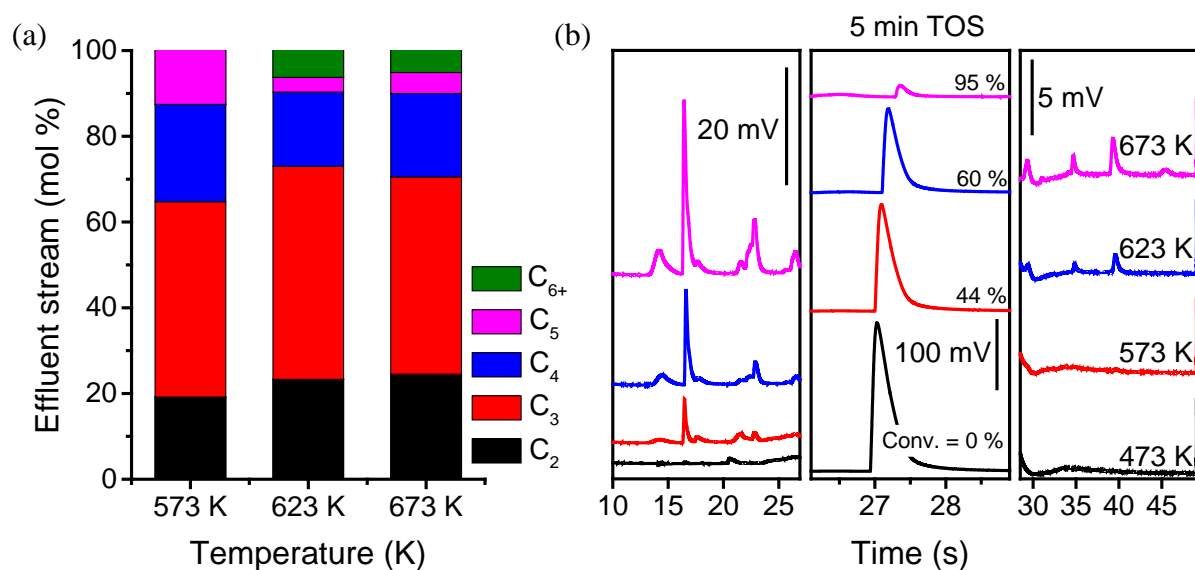


**Figure S7.** (a) Effluent stream (mol %) for the dimethylether-to-hydrocarbons reaction over HZSM-5 single crystals at different temperatures after 5 min time-on-stream (WHSV = 3.8 h<sup>-1</sup>); (b) corresponding GC traces. The catalyst was re-activated in oxygen at 823 K between each temperature measurement.

### S3. Experimental Details of Synchrotron Measurements.

#### *Operando* IR Microspectroscopy (OIMS).

A fresh batch of calcined HZSM-5 crystals were used for each IR measurement at the Diamond Light Source, MIRIAM beam line B22.<sup>7</sup> The crystals (between 1 and 3 mg) were loaded onto a CaF<sub>2</sub> window, which was placed on the heated sample stage of the modified-Linkam FTIR600 *in situ* cell (Figure S8). Although infrared spectra were measured from a single crystal at a time, we needed at least 1 mg of crystals in the cell to give sufficient sensitivity in the MS measurements. The cell has a reduced pathlength with a volume of ~50 mL. The Linkam cell was positioned onto a Bruker Hyperion 3000 microscope under a 36 X objective, coupled to a VERTEX 80 FT-IR (310) equipped with a liquid nitrogen MCT detector. Gas flow of ultra-dry nitrogen (100 mL min<sup>-1</sup>) was delivered to the cell by mass-flow controller and pulses of spectroscopic grade methanol, methanol-d<sub>3</sub> or methanol-d<sub>4</sub> (typically 4 or 8  $\mu$ L) were injected into the gas stream *via* microsyringe. Experiments with dimethylether passed a continuous flow of dimethylether (1 bar, 5 mL min<sup>-1</sup>) into the 100 mL min<sup>-1</sup> nitrogen stream. The outlet from the cell was directed to an on-line quadrupole mass spectrometer (Pfeiffer Omnistar or Ecosys portable mass spectrometer) for analysis of gas phase products.

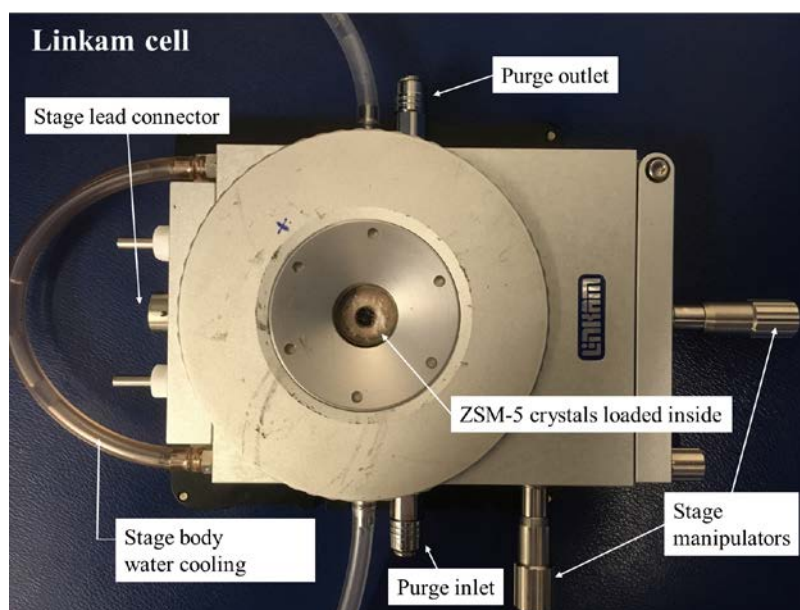


**Figure S8.** HZSM-5 crystals loaded onto a CaF<sub>2</sub> window inside the heated sample stage of the modified Linkam FTIR600 *in-situ* cell.

#### Data Acquisition.

Following sample dehydration in nitrogen (for 1 hour at 623 K), the sample stage was moved so that the microscope aperture (15  $\times$  15  $\mu$ m<sup>2</sup>) was on a crystal-free zone to collect a background spectrum. The sample stage was then moved so that the aperture was above a selected region of an individual HZSM-5 crystal and an IR spectrum was acquired.

Prior to introducing methanol into the activated (dehydrated) crystals, the spectrometer was set to collect repeat spectra over a selected crystal region with one of the following collection modes within the OPUS 7.8 Bruker software: (a) Repeated Scan (RS): This functionality records spectra by averaging 16 single-sided interferograms at 4 cm<sup>-1</sup> for each spectrum at a 2

second time resolution and a scanner velocity of 80 kHz. (b) Time-Resolved Scan (TRS): Using the rapid-scan functionality of the VERTEX 80v instrument we were able to improve the temporal resolution to 0.25 seconds / spectrum by measuring interferograms in double-sided forward/backward acquisition mode. The scanner velocity during the TRS acquisition was kept at 80 kHz at  $4\text{ cm}^{-1}$  resolution.

IR spectra were measured during the injection of methanol into fresh HZSM-5 crystals at 523–673 K under ambient pressure, or in flowing dimethylether ( $5\text{ mL min}^{-1}$ ). Spectra were recorded while continuously monitoring the gas phase reaction products with the on-line mass spectrometer. Time-zero for the FTIR and the MS data were defined as the time when the first changes were observed in each signal.

When extracting band intensities, spectra were normalised against the zeolite overtone bands at  $1800\text{-}2000\text{ cm}^{-1}$  and offset as needed.

## S4. Supplementary Infrared and MS Data.

### Crystal Homogeneity.

To test the uniformity and homogeneity of HZSM-5 crystals we recorded spectra from many different dehydrated crystals and from different spots on individual crystals, using the  $15 \times 15 \mu\text{m}^2$  aperture. Figure S9 illustrates some examples. The zeolite Brønsted acid site shows a characteristic strong band at  $3600 \text{ cm}^{-1}$ . Also evident in Figure S9 is a higher frequency  $\nu(\text{OH})$  band at  $3732 \text{ cm}^{-1}$ . This band has been attributed previously to silanol groups terminating the zeolite lattice at the external surface in conventional IR studies on macroscopic zeolite samples.<sup>7</sup> This assignment is unlikely in our case as the contribution of silanol groups on the external surfaces of large individual crystals will be negligible relative to the contributions from internal hydroxyl groups. A more likely interpretation of the silanol band is that it is due to lattice defects. Large ZSM-5 crystals are known to comprise intergrowths of two different orientations of the  $a$  and  $b$  axes of the crystal (giving a characteristic hour glass pattern in optical micrographs, as seen in Figure S1), and the interfaces between these intergrowths will contain silanol groups. We could not distinguish any differences in relative populations of silanol groups in different regions of individual crystals and the intensities of the Brønsted acid  $\nu(\text{OH})$  bands were remarkably constant in all regions and crystals sampled. The bands at  $1995$ ,  $1870$  and  $1630 \text{ cm}^{-1}$  in the above figure are due to overtones and combination bands of the lower frequency Si-O-Al stretching and bending modes of the zeolite framework.<sup>8,9</sup> In all of the spectra reported subsequently (and in the main article) are difference spectra; the spectrum of the dehydrated zeolite has been subtracted from the spectra measured subsequent to methanol adsorption. The strong lattice bands below  $1400 \text{ cm}^{-1}$  preclude any measurements in this region.

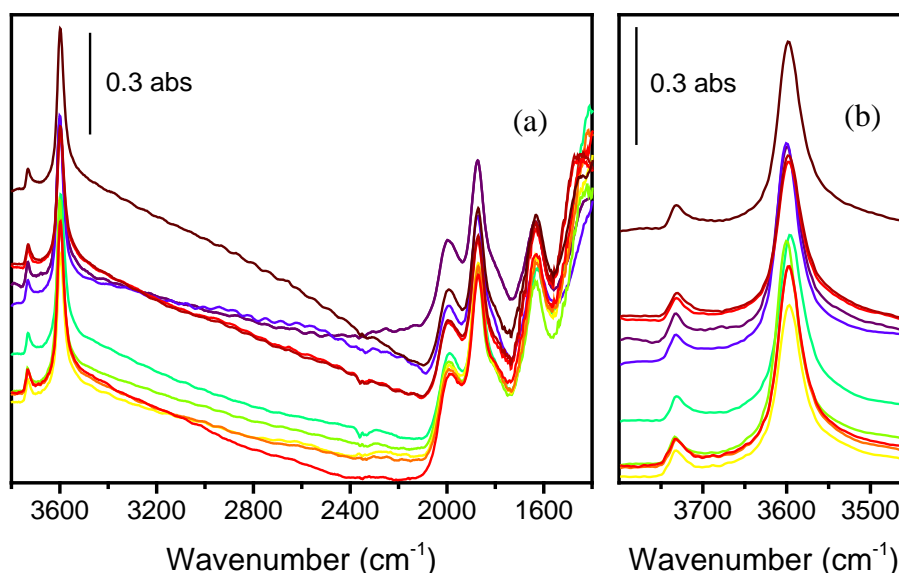


**Figure S9.** (a) FTIR spectra of dehydrated HZSM-5 zeolite measured from different crystals (at  $623 \text{ K}$ ); (b) Expansion of the  $\nu(\text{OH})$  region.

## Infrared Difference Spectra of the First Methanol Pulse in HZSM-5 Crystal at 573 K.

Figure S10 shows difference spectra recorded at 2 s intervals when an 8  $\mu\text{L}$  pulse of methanol is passed over a HZSM-5 crystal at 573 K. The final spectrum (in red) was recorded 30 s after the first methanol was detected by MS in the effluent stream. The spectra show a progressive decrease in the zeolite  $\nu(\text{OH})$  mode and the growth of the ABC triplet characteristic of hydrogen bonded methanol and dimethylether. Closer examination of the  $\nu(\text{CH})$  region shows that although methanol may be present in the first few scans the later spectra show the bands of hydrogen bonded dimethylether. This can be seen from comparison with spectra obtained when methanol and dimethylether were adsorbed into a ZSM-5 crystal at 473 K.

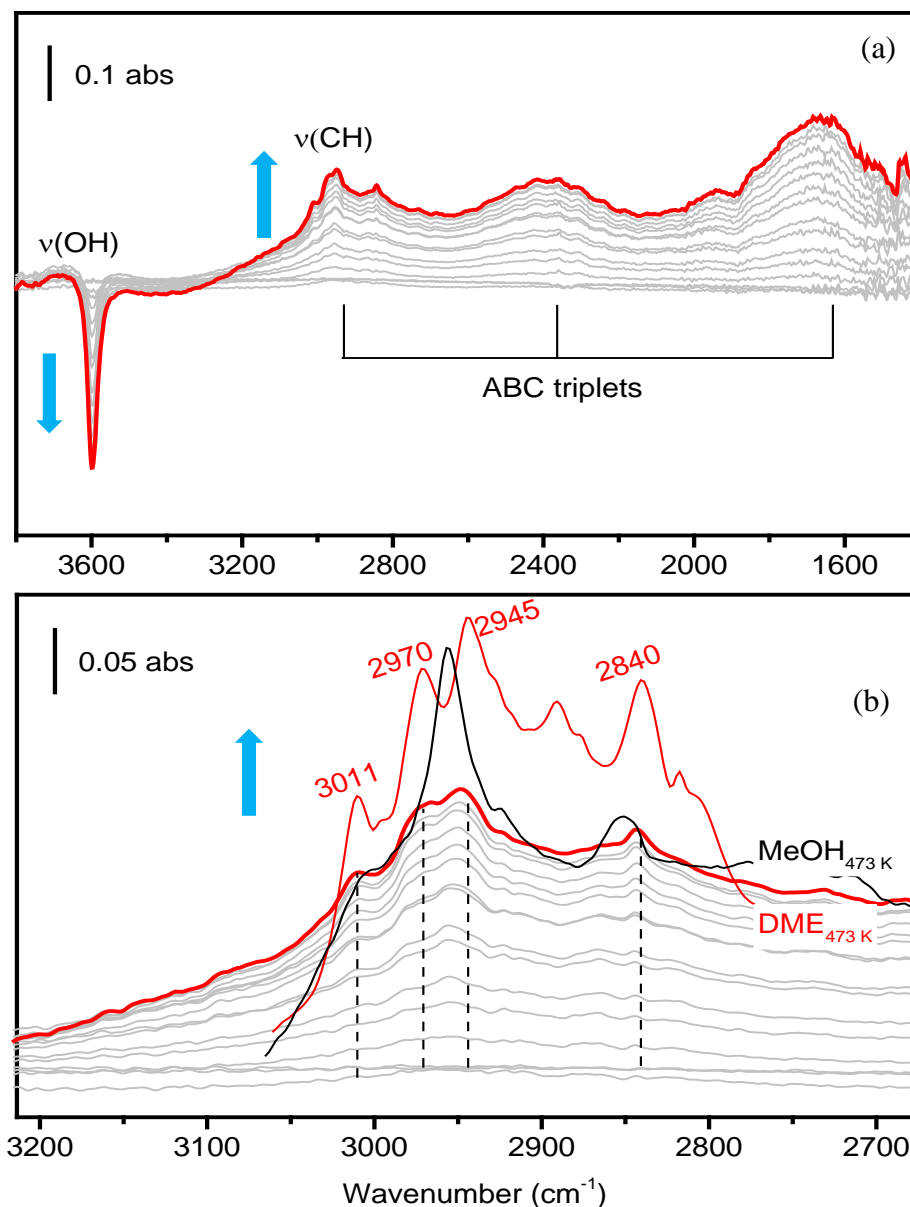


**Figure S10.** (a) Difference spectra recorded at 2 s intervals for 30 s following injection of an 8  $\mu\text{L}$  pulse of methanol into a HZSM-5 crystal at 573 K. (b) expansion of CH stretching region and comparison with spectra of methanol and dimethylether adsorbed in HZSM-5 at 473 K. Arrows indicate direction of change.

### Blank MS Profile of 8 $\mu\text{L}$ $\text{CD}_3\text{OH}$ Pulse into an Empty Cell at 573 K versus $\text{CD}_3\text{OH}$ Reacting in HZSM-5 at 573 K.

Figure S11(a) shows MS profiles recorded when a pulse of methanol- $\text{d}_3$  was injected into the Linkam cell held at 573 K containing no zeolite crystals. The  $m/z = 50$  peak of DME- $\text{d}_6$  is more than an order of magnitude lower than that seen in the presence of zeolite crystals (Fig S11(b)); evidently some dehydration of methanol can occur on the hot surfaces of the cell. The  $m/z = 48$  peak can be due to fragmentation of DME- $\text{d}_6$  and the  $m/z = 47$  peak to fragmentation of DME- $\text{d}_5$ , but these are barely above the baseline detection limits on the logarithmic scale used. The only possible source of traces of DME- $\text{d}_5$  is a methanol- $\text{d}_2$  impurity in the methanol- $\text{d}_3$ . In the presence of zeolite crystals (Figure S11(b)) the  $m/z = 47$  and  $m/z = 48$  peaks coincident with DME are at the same levels as in the blank, but increase by up to an order of magnitude at the point where the OD groups appear.

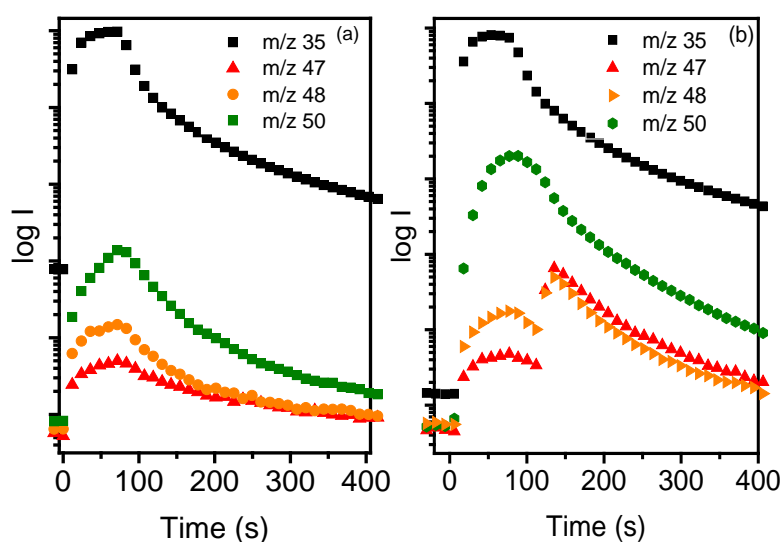


**Figure S11.** (a) MS profile of the blank 8  $\mu\text{L}$   $\text{CD}_3\text{OH}$  injection into an empty cell in nitrogen flow ( $100 \text{ ml min}^{-1}$ ) at 573 K. (b) 8  $\mu\text{L}$   $\text{CD}_3\text{OH}$  injection into cell containing  $150 \times 60 \times 60 \mu\text{m}^3$  HZSM-5 crystals in nitrogen flow ( $100 \text{ ml min}^{-1}$ ) at 573 K. In this case after 110 seconds,  $m/z = 35$  measures  $\text{CD}_3\text{OH}$ ,  $m/z = 50$  measures  $\text{CD}_3\text{OCD}_3$ ,  $m/z = 48$  measures propene- $\text{d}_6$  (with a contribution from fragmentation of  $\text{CD}_3\text{OCD}_3$ ),  $m/z = 47$  measures propene- $\text{d}_5$  (with a contribution from fragmentation of  $\text{CD}_3\text{OCHD}_2$ ).

### HZSM-5 Crystal Exposed to Ethene at 473 K then Heated in Nitrogen to 573 K.

Figure S12 shows the formation of oligomeric species (2960, 2870  $\text{cm}^{-1}$ ) and the growth of adsorbed DMCP cation (1510, 1460  $\text{cm}^{-1}$ ) with time on stream in HZSM-5 exposed to an ethene pulse ( $\sim 600$  s) at 473 K. Note that gas phase ethene is present as weak bands around 3100  $\text{cm}^{-1}$ . These are immediately lost when the ethene flow is stopped. Also present is a band at  $\sim 3450$   $\text{cm}^{-1}$  due to perturbation of zeolite OH groups by interaction with the oligomer. Upon heating to 573 K in flowing nitrogen (100  $\text{ml min}^{-1}$ ),  $m/z$  41 and  $m/z$  55 evolve in the gas phase products from cracking of the oligomeric species. The blue trace in Figure S13 (a) is the spectrum after it was flushed in nitrogen at 573 K showing adsorbed DMCP species. (see below).

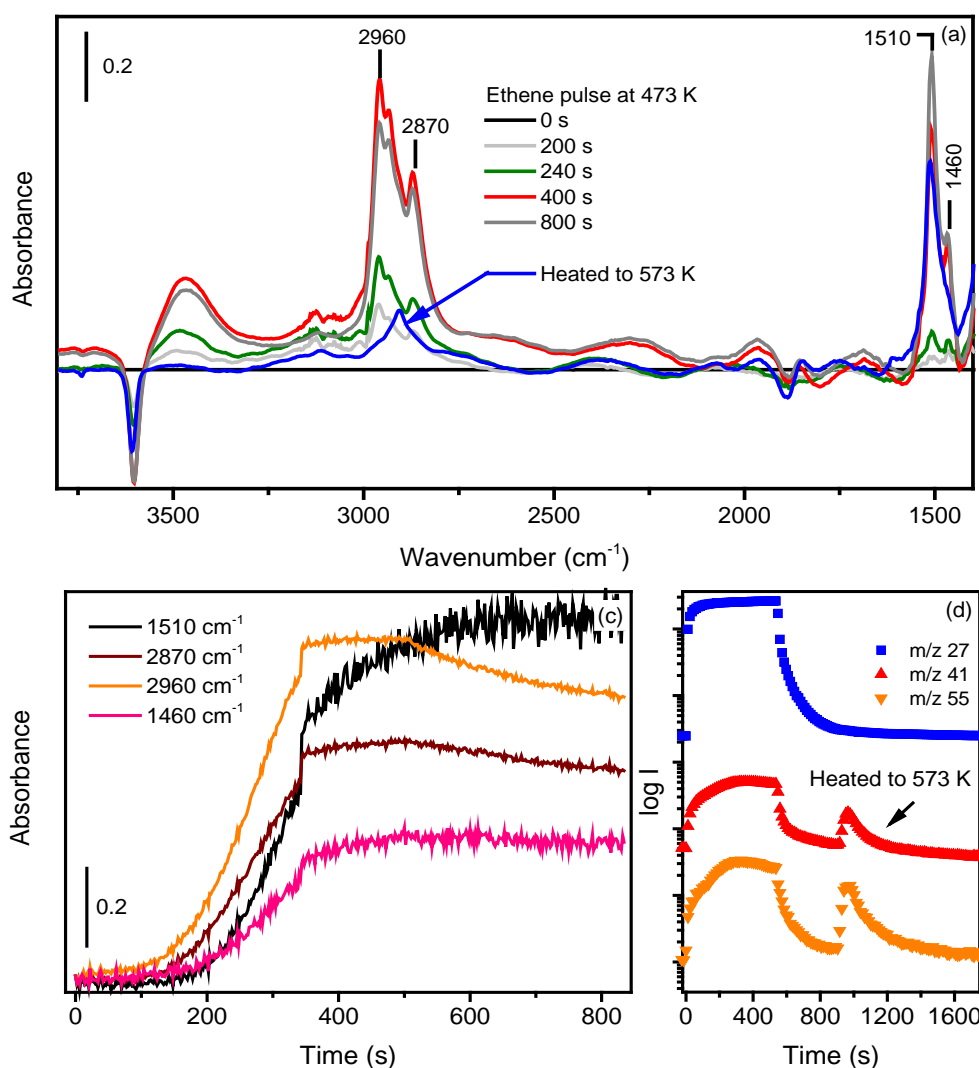


**Figure S12.** (a) Infrared difference spectra recorded following exposure of a  $150 \times 60 \times 60 \mu\text{m}^3$  HZSM-5 crystal to a continuous flow (over 500 s) of ethene at 473 K crystal, and after heating in flowing nitrogen to 573 K (blue); (b) Intensity of 2960, 2870, 1510 and 1460  $\text{cm}^{-1}$  bands versus time during the same experiment; (c) corresponding MS analysis of effluent gas stream.  $m/z = 27$  measures ethene;  $m/z = 41$  measures propene,  $m/z = 55$  measures butene.

### Spectra of the 1,3-dimethylcyclopentenyl Cation.

Figure S11 compares the infrared difference spectra of the 1,3-dimethylcyclopentenyl cation obtained from ethene, propene, dimethylether, methanol and methanol-d<sub>4</sub> reacted over a crystal of HZSM-5. In (a) the spectrum obtained from ethene was measured at 523 K after injecting a 42 mL pulse of ethene at 473 K and then flushing in nitrogen for 400 s at 573 K. In (b) the spectrum obtained from propene was measured 400 s after injecting a 2 mL pulse of propene at 523 K. At this temperature, ethene and propene forms oligomer species, see Figure S12 and Figure 3 in the paper, but by 400 s after flushing in nitrogen these have been completely removed and the spectrum plotted in (a) and (b) is that of the 1,3-dimethylcyclopentenyl cation. In (c), the spectrum from dimethylether was generated by exposing an HZSM-5 crystal to a continuous flow of dimethylether (5 mL min<sup>-1</sup>) at 573 K for 700 s. The  $\nu(\text{CH})$  region of this spectrum shows some oligomer species still present, but the features of 1,3-dimethylcyclopentenyl cation dominate. The spectra from methanol in (d) and methanol-d<sub>4</sub> in (e) were measured after injection of three successive 8  $\mu\text{L}$  pulses and likewise contain also small contributions from oligomer. Note that the spectrum obtained from methanol-d<sub>4</sub> also shows the presence of a weak  $\nu(\text{CH})$  band at 2910 cm<sup>-1</sup> due to exchange with zeolite OH groups, while the strong band at 2630 cm<sup>-1</sup> is due to zeolite OD groups. Traces of the 1620 cm<sup>-1</sup> band assigned to methylaromatic species are present in all spectra in varying amounts (this band is also shifted by  $\sim 20$  cm<sup>-1</sup> to lower frequency when formed with methanol-d<sub>4</sub>). The boxed region between 2000 and 1700 cm<sup>-1</sup> contains artefacts due to subtraction of zeolite lattice overtone bands which have been perturbed by adsorption. Table S2 compares the frequencies of the bands assigned here to the 1,3-dimethylcyclopentenyl cation with those reported for the gas phase species.

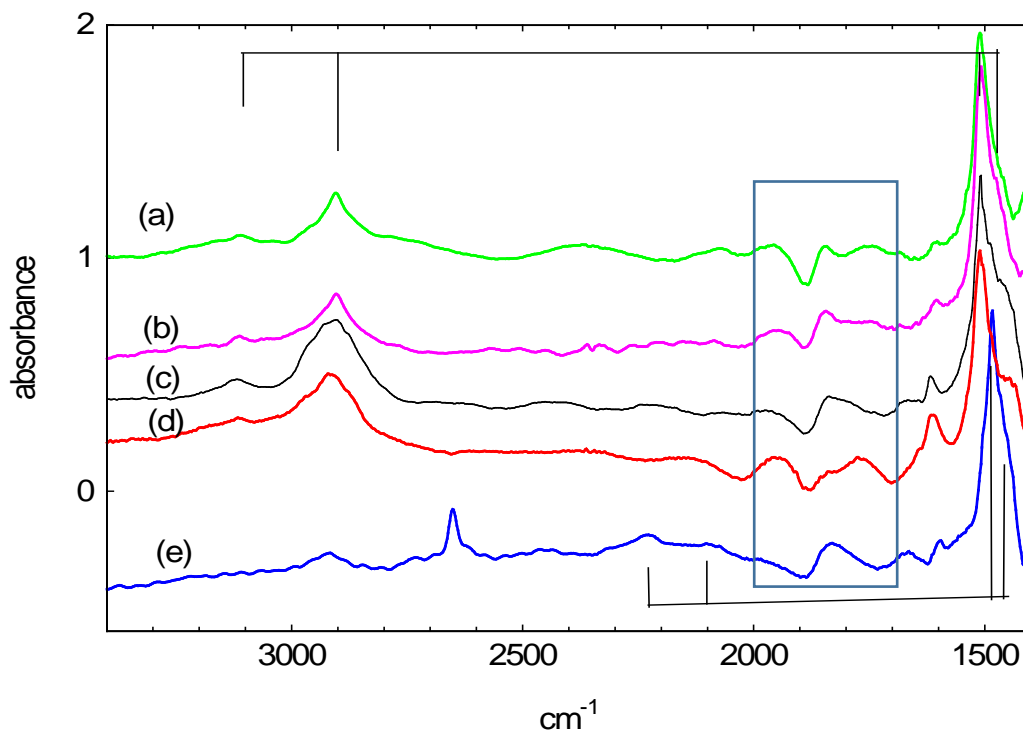


**Figure S13.** Infrared difference spectra of the dimethylcyclopentenyl cation formed from (a) ethene (b) propene, (c) dimethylether, (d) methanol and (e) methanol-d<sub>4</sub> in HZSM-5 crystals.

**Table S2.** Infrared frequencies of 1,3-dimethylcyclopentenyl cation (DMCP) in HZSM-5 formed from different molecules (propene, dimethylether, methanol and methanol-d<sub>4</sub>).

Gas phase DMCP*	Vibrational modes DMCP*	C <sub>3</sub> H <sub>6</sub>	CH <sub>3</sub> OCH <sub>3</sub>	CH <sub>3</sub> OH	CD <sub>3</sub> OD
<b>3101</b>	Allyl ν(CH)	3114	3116	3110	2217
<b>3017, 2995</b>	CH <sub>3</sub> , CH <sub>2</sub> asymm str.	Not resolved	Not resolved	Not resolved	Not resolved
<b>2910</b>	CH <sub>3</sub> , CH <sub>2</sub> symm str.	2905	2908	2910	2080
<b>1525</b>	Allyl CCC asym.str.	1510	1510	1510	1482
<b>1482</b>	Allyl CCC symm str.	1475 (shoulder)	1465 (shoulder)	1460 (shoulder)	Not resolved
<b>1421</b>	CH <sub>3</sub> asymm.bend	Not resolved	Not resolved	Not resolved	Not resolved

\*Mosley J.D.; Young J.W.; Agarwal J.; Schaefer H.F.; Schleyer P.R.; Duncan M.A. Structural isomerization of the gas-phase 2-norbornyl cation revealed with infrared spectroscopy and computational chemistry, *Angew.Chem.Int.Ed.* **2014**, *53*, 5888-5891.

## Methanol Pulses in HZSM-5 Crystals of Different Size at 623 K.

Figure S14 shows the intensities of the  $1510\text{ cm}^{-1}$  and  $1620\text{ cm}^{-1}$  bands discussed in the text as a function of time during injection of three successive pulses of methanol into two different sizes of HZSM-5 crystals at 623 K. Figure S12(a) and the corresponding MS data in (b) refer to a crystal of similar size to those described in the paper ( $150 \times 60 \times 60\ \mu\text{m}^3$ ). (c) and the MS data in (d) to a crystal of smaller size ( $60 \times 30 \times 30\ \mu\text{m}^3$ ). The data show that there is no correlation between the intensities of the  $1510\text{ cm}^{-1}$  band (assigned to the DMCP cation) and the  $1620\text{ cm}^{-1}$  band assigned to adsorbed methylaromatic species. There is no induction period in the appearance of alkenes at this temperature, and in comparing the two sizes of crystal there is a correlation between the intensity of the  $1620\text{ cm}^{-1}$  band and the yield of methyl aromatic products ( $m/z = 91$  peak is due to the tropylium cation, a major fragment in the mass spectra of methyl aromatic molecules). The smaller crystals are more reactive, due to the shorter diffusion paths.

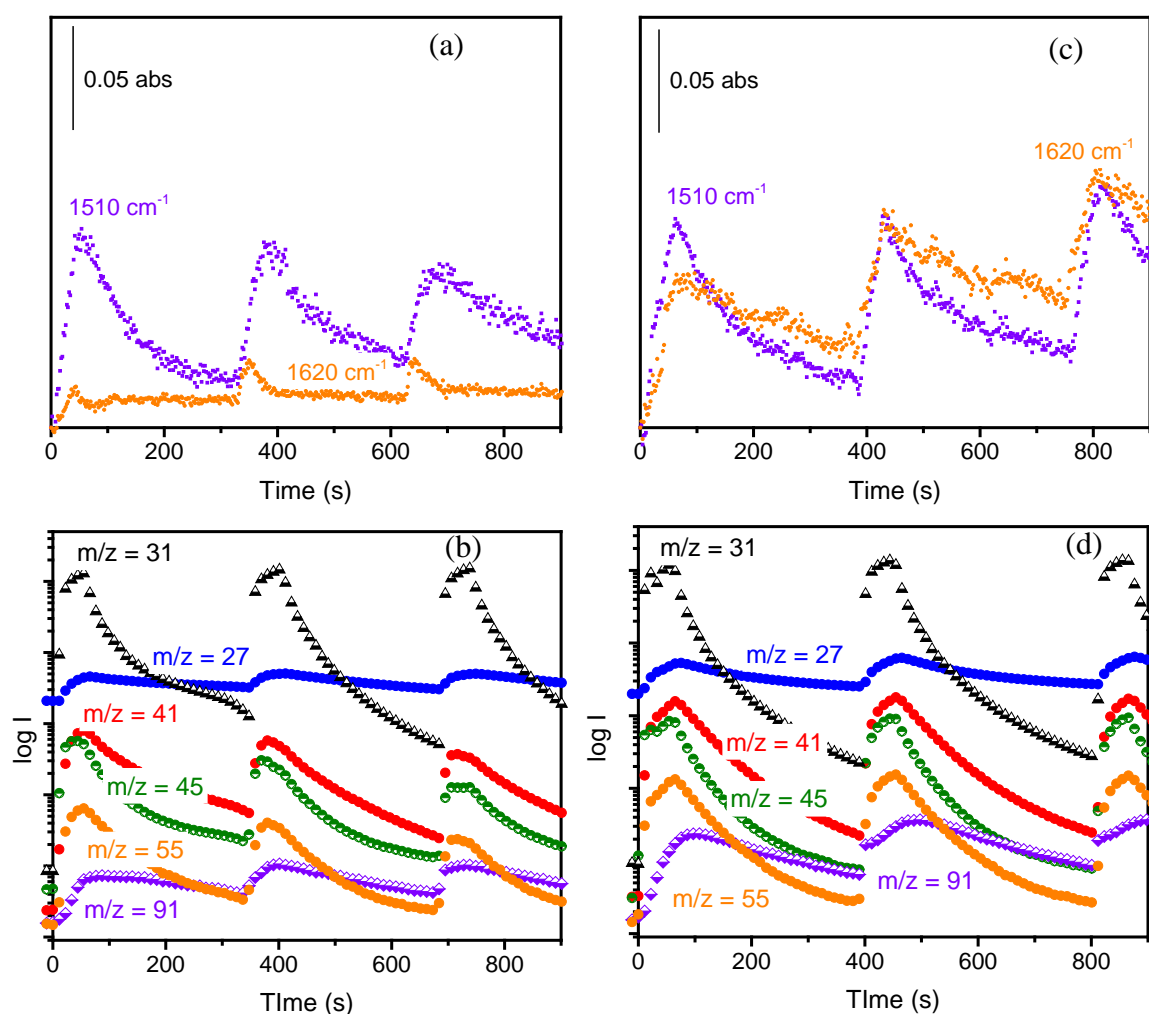


**Figure S14.** (a), Intensity of  $1510\text{ cm}^{-1}$  and  $1620\text{ cm}^{-1}$  versus time during injection of three successive  $8\ \mu\text{L}$  pulses of methanol into a  $150 \times 60 \times 60\ \mu\text{m}^3$  HZSM-5 crystal at 623 K; (b) corresponding MS analysis of effluent gas stream.  $m/z = 31$  measures methanol;  $m/z = 27$  measures ethene;  $m/z = 41$  measures propene,  $m/z = 45$  measures dimethylether;  $m/z = 55$  measures butene;  $m/z = 91$  measures methyl aromatics. (c) and (d): data from the same experiment with a smaller crystal ( $60 \times 30 \times 30\ \mu\text{m}^3$ ).

### HZSM-5 Crystal Exposed to a Continuous Flow of Dimethylether at 623 K.

Exposure of a HZSM-5 crystal to a continuous flow of dimethylether at 623 K caused immediate appearance of the bands attributed to the DMCP cation which then decayed, as illustrated in Figure S15. The time dependence of the 1510  $\text{cm}^{-1}$  band of DMCP correlated well with the MS signals of ethene, propene and butene, supporting our suggestion that cracking of the DMCP is a major source of alkenes. The 1620  $\text{cm}^{-1}$  band, on the other hand, grew continuously in intensity over 800 s of exposure to dimethylether, and the MS signal of the methyl aromatic products rose more slowly, then remained constant. The spectra recorded at later stages of dimethylether exposure at this temperature showed the appearance of number of other weaker bands between 1620 and 1450  $\text{cm}^{-1}$  consistent with formation of the more complex mixture of species associated with the steady state hydrocarbon pool.

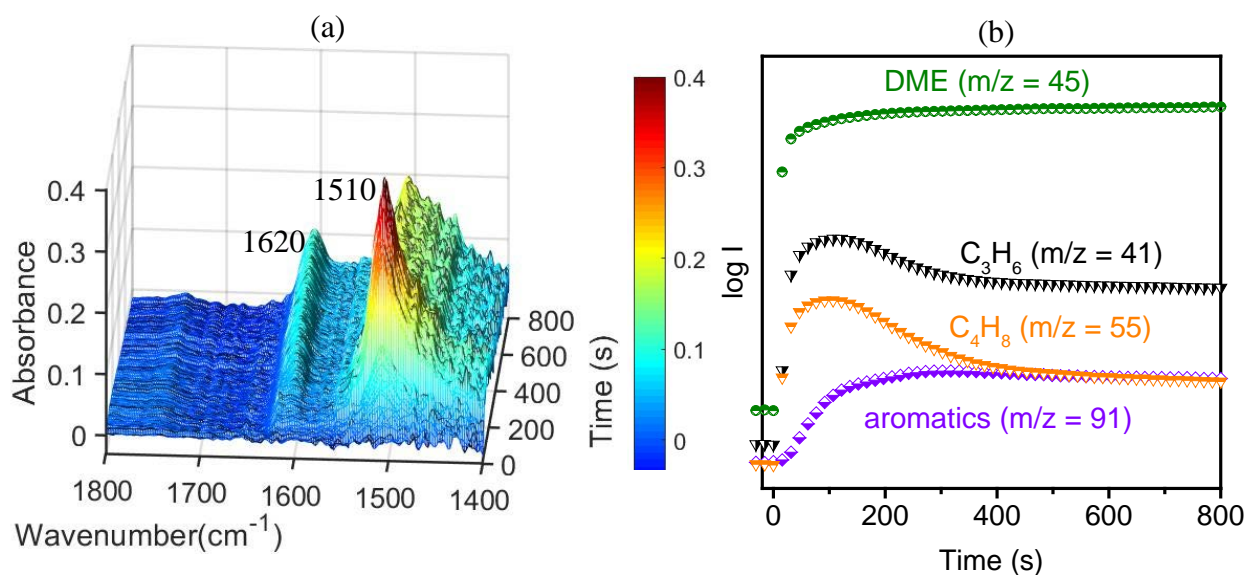


**Figure S15.** (a) Infrared spectra recorded at 2 s intervals following exposure of a  $150 \times 60 \times 60 \mu\text{m}^3$  HZSM-5 crystal to a continuous flow of dimethylether at 623 K, showing the initial growth and then decay of the dimethylcyclopentenyl cation species ( $1510 \text{ cm}^{-1}$ ), and growth of adsorbed aromatic species ( $1620 \text{ cm}^{-1}$ ) with time on stream; (b) mass spectral traces of evolved products, showing rise and decline of alkenes compared with  $1510 \text{ cm}^{-1}$  band, and growth of methylaromatic products compared with rise in  $1620 \text{ cm}^{-1}$  band.

## Infrared Spectra of Methylacetate Injected into an HZSM-5 Crystal

At 573 K, methyl acetate is initially H-bonded to the zeolite acid site, as seen by the A and B components of the hydrogen bonding triplet. Evident also in the initial spectra at  $\sim 1750\text{ cm}^{-1}$  are carbonyl  $\nu(\text{C}=\text{O})$  bands of gas phase methylacetate. An intense vibrational band of methyl acetate is seen at  $1674\text{ cm}^{-1}$  together with the adsorbed methyl acetate  $\nu(\text{CH})$  vibration at  $2960\text{ cm}^{-1}$ . Such bands were not evident in the methanol experiments, and confirm the absence of carbonyl containing species during the formation of olefins at 573 K. At the trailing edge of the third pulse (blue trace), many new bands are seen which were not present at the corresponding stage of methanol experiments, indicating a different hydrocarbon pool composition.

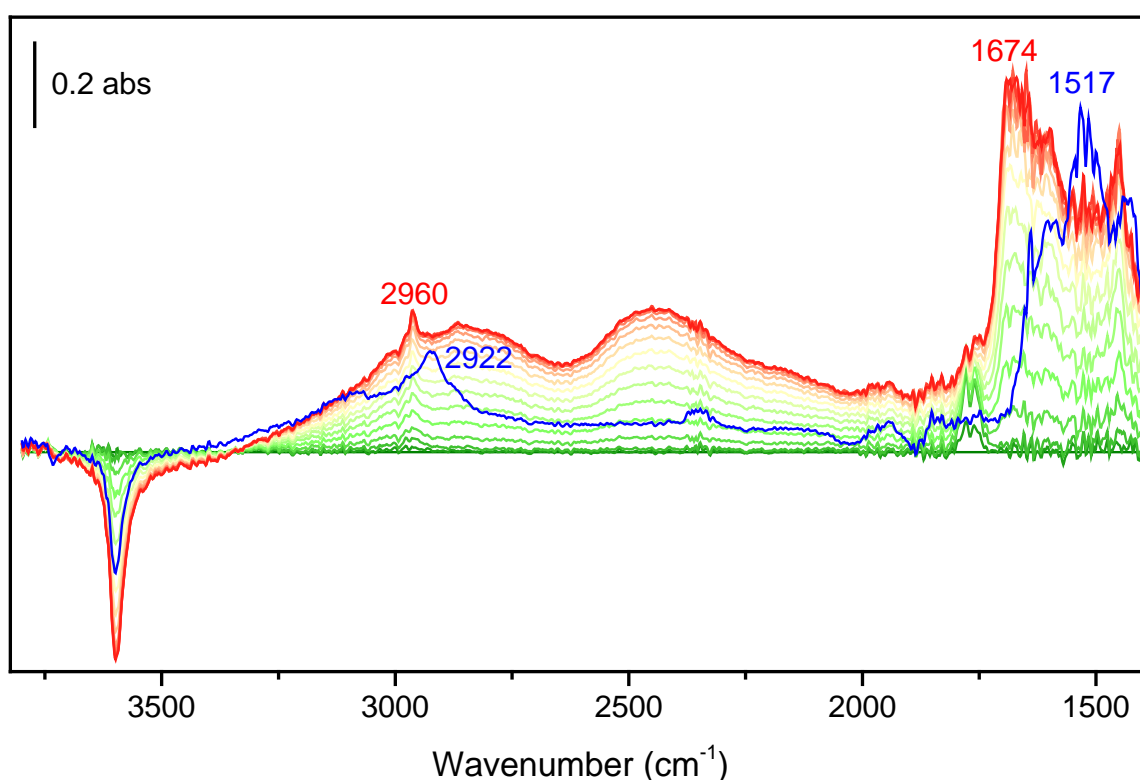


**Figure S16.** Difference FTIR spectra following injection of an  $8\ \mu\text{L}$  methylacetate-pulse into a  $150 \times 60 \times 60\ \mu\text{m}^3$  HZSM-5 crystal at 573 K and overlaid (in blue) is the difference FTIR spectrum obtained immediately after three successive  $8\ \mu\text{L}$  methylacetate pulses at 573 K.

## References

- (1) Guth J.L.; Kessler H.; Wey R.; Murakami Y.; Iijima A.; Ward J.W. New Route to Pentasil-Type Zeolites Using a non Alkaline Medium in the Presence of Fluoride Ions *Studies in Surface Sci. and Catal.*, **1986**, 28, 121-128.
- (2) Losch P.; Pinar A.B.; Willinger M.G.; Soukup K.; Chavan S.; Vincent B.; Pale P.; Louis B. H-ZSM-5 Zeolite Model Crystals: Structure-Diffusion-Activity Relationship in Methanol-to-Olefins Catalysis, *J. Catal.* **2017**, 345, 11–23.
- (3) Jackson, K.T.; Howe R.F. Studies of Zeolite Single-Crystals: Ethene Oligomerization in H-ZSM-5, *Stud. Surf. Sci. Catal.* **1994**, 83, 187-194.
- (4) Ristanovic Z.; Hofmann, J.P.; Deka, U.; Schüllli, T.U.; Rohnke, M.; Beale, A.M.; Weckhuysen B.M. Intergrowth Structure and Aluminium Zoning of a Zeolite ZSM-5 Crystal as Resolved by Synchrotron-Based Micro X-Ray Diffraction Imaging. *Angew. Chem. Int. Ed.* **2013**, 52, 13382 –13386.
- (5) Sazama, P.; Wichterlova B.; Dedecek J.; Tvaruzkova Z.; Musilova Z.; Palumbo L.; Sklenak S.; Gonsiorova O. FTIR and  $^{27}\text{Al}$  MAS NMR Analysis of the Effect of Framework Al- and Si-defects in Micro- and Micro-Mesoporous H-ZSM-5 on Conversion of Methanol to Hydrocarbons *Micro. and Meso. Materials* **2011**, 143 87-96.
- (6) Sarv, P.; Fernandez, C.; Amourex, J.; Keskinen, K.J. Distribution of Tetrahedral Aluminium Sites in ZSM-5 Type Zeolites: An  $^{27}\text{Al}$  (Multi-quantum) Magic Angle Spinning NMR Study *Phys. Chem.* **1996**, 100 19223-19226.
- (7) Cinque, G.; Frogley, M.D.; Wehbe, K.; Filik, J.; Pijanka, J. Multimode InfraRed Imaging and Microspectroscopy (MIRIAM) Beamline at Diamond, *Synchrotron Rad. News* **2011**, 24, 24-33.
- (8) Yamagishi, K.; Namba, S.; Yashima, T. Defect Sites in Highly Siliceous HZSM-5 Zeolites: A Study Performed by Almination and IR Spectroscopy. *J. Phys. Chem.* **1991**, 91, 872-877.
- (9) Peuker Ch.; Splett Ch. Overtone and Combination Tone Bands in the DRIFT Spectra of Molecular sieves. *J. of Molecular Structure*, **1993**, 294, 23 1-234.